Hindawi
Geofluids
Volume 2022, Article ID 8214322, 11 pages
https://doi.org/10.1155/2022/8214322

Research Article

Quantitative Study on the Stress Distribution Characteristics of Coal Rock with Faults

Dayang Xu,[1,2] Hu Si,[1,2] Qianting Hu,[1,2] and Yunpei Liang[1,2]

[1]*State Key Laboratory of Coal Mine Disaster Dynamics and Control, Chongqing University, Chongqing 400044, China*
[2]*School of Resources and Safety Engineering, Chongqing University, Chongqing 400044, China*

Correspondence should be addressed to Hu Si; sihu@cqu.edu.cn

Received 23 December 2021; Accepted 5 February 2022; Published 28 February 2022

Academic Editor: Yue Niu

To quantitatively describe the distribution characteristics of stress field of coal rock in fault area, a finite element model was established to study the influence mechanisms of different fault parameters on the stress distribution characteristics of coal rock and a prediction model of the tectonic stress field of a fault-containing coal rock was established based on the numerical simulations. The numerical simulation results show that the coal rock in the hanging wall of a normal fault forms an area of disturbance significantly larger than that in the footwall of the normal fault and reverse fault. With the increase in fault throw, the stress concentration factor and fault influence range decrease in both the normal and reverse fault scenarios. Additionally, for both the normal and reverse fault scenarios, with the increase in fault dip angle, the coal rock stress concentration zone gradually collapses to the fault plane and the stress concentration coefficient gradually increases due to the reduction in the area of pressure relief. The prediction model of the tectonic stress field can better describe the quantitative relationship between the fault parameters and the stress of coal rock, which can provide guidance for the excavation design of mining engineering and early warning for possible coal and gas outburst disasters.

1. Introduction

Coal and gas outbursts are serious dynamic disasters that can occur during coal mining. Coal and gas outbursts are essentially mechanical destruction processes and are closely related to the geological structure [1–3]. Research suggests that a large number of fissures develops and a high concentration of in situ stress arises near small faults in a mining area, which changes the physical and mechanical properties of coal and rock mass, creating the conditions for mechanical damage and possible coal and gas outbursts; this is the main geological factor affecting the distribution of coal and gas outbursts in the mining area [4–15]. Therefore, it is of great significance to study the stress distribution of coal rock with faults for the prediction and prevention of coal and gas outbursts and to guide safe mining practices in coal mines.

In situ measurement of in situ stress is the most direct way to study the tectonic stress field around faults, but it is easily restricted due to the complex and changeable conditions, the long test cycles, and the high costs of in situ tests [16–19]. In addition, in situ measurements can describe only the local in situ stress, and a limited amount of measurement data cannot accurately reflect the regional stress field, making it difficult to meet the needs of mine engineering design and construction. In view of this, measured in situ stress data have been gradually applied to the inversion analysis of the tectonic stress field around faults to more accurately estimate the in situ stress in the fault region with limited measurement data [20–24]. With the development of computer hardware and software, numerical simulation methods have been increasingly widely used in the study of tectonic stress because of the shorter research periods required, more intuitive research results, and less limited field environment. At present, numerical simulation methods of coal and rock mass have been widely used in the study of the stress fields at fault tips [25–28] and fault group [29], stability analysis of surrounding rock near faults [30–36], influence

mechanism of fault parameters on the degree of disturbance to the stress field [37–39], etc.

In the existing research on tectonic stress fields around faults, most of the research objects are large fault zones, while few studies have focused on a single small fault, which are the main geological factors affecting the distribution of coal and gas outbursts. The previous research results mainly focus on the discussion and analysis of the mining-disturbed stress field under specific engineering problems, while research on the original rock stress field before mining is relatively lacking, and the influence mechanism of various fault parameters on the in situ stress distribution of coal and rock mass near small faults is not well discussed and summarized. The existing research results provide some qualitative conclusions, but for preventing coal and gas outbursts in practice, quantitative conclusions are more desirable. Even if a quantitative conclusion has certain errors and limitations, as long as it is within the acceptable range, it can greatly promote the development of outburst prevention technology.

Based on the principles of continuum mechanics and finite element numerical simulation methods, this study establishes a two-dimensional finite element model of a coal rock with a fault and studies the stress distribution characteristics of coal rock under the influence of different fault parameters. Then, based on the numerical simulation data and supervised learning artificial neural network, a prediction model of the tectonic stress field of a fault-containing coal rock is established to quantitatively characterize the mapping relationship between the stress of coal rock at various points near the fault and their spatial location and the fault property, throw, and dip angle.

2. Finite Element Calculation Model

2.1. Mechanical Model. To avoid obtaining a solution that is too complicated, the calculation model was simplified as follows: (1) the coal and rock mass around the fault was a homogeneous isotropic material. (2) The medium of the fault fracture zone was regarded as a completely elastic material. (3) All the rock layers were oriented horizontally, and the boundary stress was applied perpendicular to the boundary. (4) The geological model was simplified to a plane strain model. A Drucker–Prager constitutive model was adopted for each material, and the rock mechanical parameters required for calculation are listed in Table 1.

2.2. Geometric Models and Boundary Conditions. According to the movement relationship between the hanging wall and footwall of the fault, two-dimensional geometric models were established, one with a normal fault and one with a reverse fault, as shown in Figure 1, respectively. The overall size of the model was 400 m × 100 m, and the width of the fault fracture zone was 2 m. The thickness of each rock layer on the left side of the fault is listed in Table 1, while each rock layer on the right side had a throw of 2 m from the left. The boundary conditions imposed by the models are indicated in Figure 1. The normal and reverse fault models were applied with horizontal stress of 2.7 MPa and 11 MPa, respectively, while the gravity of the overlying rock was applied to both in the vertical direction of 8 MPa. The purpose of this study was to investigate the distribution characteristics of the tectonic stress field, so the gravity of the model itself was not considered.

2.3. Model Validation. To verify the reliability of the numerical model, the stress near the fA42 fault in the #11 gas drainage roadway of the Shihao coal mine was measured at multiple points, and a finite element calculation model was established under the same working conditions. The fA42 fault had an occurrence of N16°E ∠ 65°, with a drop of 2 m and a fracture zone width of 2 m. Four groups of in-situ stress measuring points were located in the limestone of M8 coal seam floor, and their corresponding positions in the numerical model were located in the limestone at $y = 15$ m. A comparison between the simulated stress and the measured stress results at each measuring point is shown in Figure 2. Although the results at each measurement point are somewhat different due to the simplification of the numerical model, the overall trend of the numerical results is basically consistent with the distribution of the measured results, which can be used as a reference for the correctness of the numerical model to a certain extent.

3. Stress Distribution Characteristics of Coal Rock with Faults

The area corresponding to a stress higher than (lower than) 5% of the original rock is divided into a stress concentration zone (stress release zone). To quantitatively describe the influences of different fault parameters on the initial stress field of coal rock, the influence range D of the fault on the stress field of the coal rock and the stress concentration coefficient k are introduced, where D is defined as the distance between the boundary of the stress zone of the original rock and the fault plane, and k is defined as the ratio of the peak stress in the stress concentration zone to the original stress.

3.1. Influence of a Normal Fault on the Stress of Coal Rock

3.1.1. Different Throws. Figure 3 shows the maximum principal stress distribution of the coal rock in the hanging wall and footwall of a normal fault with the distance L from the fault under different throws d. The results show that the stress of the coal rock in the hanging wall mainly increases within 100 m from the fault plane, reaching the maximum value 40 m from the fault, and gradually decreases to the original stress away from the fault. When the fault slip increases from 1 m to 15 m, both the k and D of the hanging wall decrease accordingly; the k is less than 1.1 under those throw conditions, and the D is reduced from 71 m to 65 m. The footwall coal rock mainly produces a stress release zone within 60 m from the fault plane, which reaches the minimum value at the fault plane and gradually increases to the original rock stress away from the fault. When the fault

Table 1: Mechanical properties of rock masses.

Lithology	Elastic modulus (GPa)	Poisson ratio	Cohesion (MPa)	Internal friction angle (°)	Density (kg·m^{-3})	Thickness (m)
Sandstone	14.14	0.25	7.00	37.8	2560	38
Mudstone 1	2.73	0.29	7.21	37.4	2660	6
Coal	1.20	0.35	1.50	32.0	1440	3
Mudstone 2	2.34	0.29	5.74	38.2	2740	4
Limestone	12.91	0.25	6.55	39.1	2619	49
Fault	0.3	0.35	—	—	1800	2

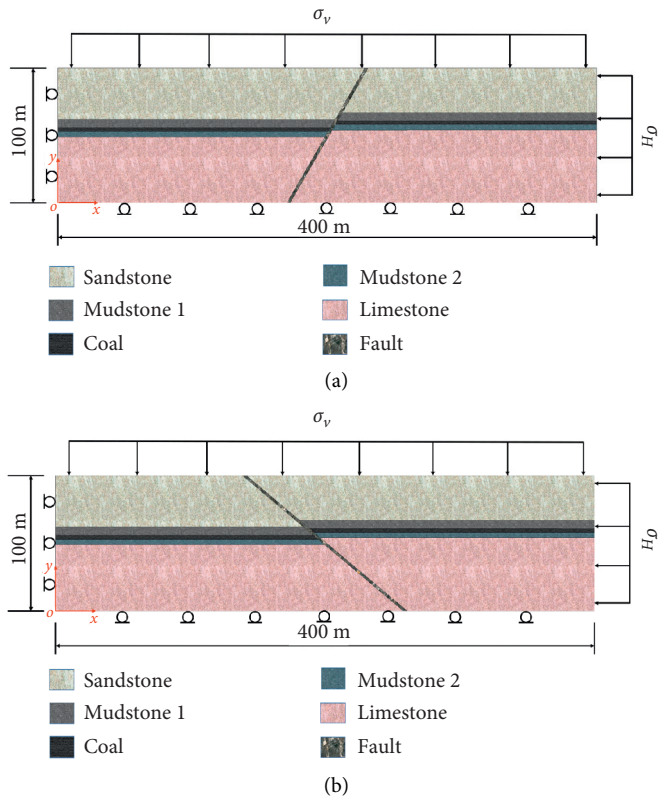

Figure 1: Geometric models with normal fault (a) and reverse fault (b).

throw gradually increases from 1 m to 15 m, the D of the footwall decreases from 26 m to 16 m.

3.1.2. Different Dip Angles. Figure 4 shows the maximum principal stress distribution of the coal rock in the hanging wall and footwall of a normal fault under different dip angles θ. The results show that the stress release zone and the stress concentration zone appear successively in the hanging coal rock away from the fault and that the initial stress is maintained in the original rock stress zone. With the increase in the dip angle, the stress release zone of the coal rock in the hanging wall gradually shrinks until it disappears, while the stress concentration zone moves closer to the fault plane. When the dip angle increases from 30° to 80°, the k of the coal rock in the hanging wall presents a trend of first increasing and then decreasing and reaches its maximum value at a dip angle of 70°. The D of the coal rock in the hanging wall decreases gradually from 136 m to 37 m with increasing dip angle. The footwall coal rock has mainly a high-stress gradient in the area within 30 m from the fault plane, which generally decreases first and then increases away from the fault. When the dip angle increases from 30° to 40°, the footwall coal rock mainly produces a stress concentration zone within 10 m from the fault plane, and the k decreases with increasing dip angle. When the dip angle continues to increase, the footwall coal rock mainly produces a stress release zone near the fault plane, and the stress gradually increases to the original stress far from the fault. The D of the coal rock in the footwall is approximately 30 m near the fault plane; it first increases and then decreases with increasing dip angle and reaches its maximum value of 28 m when the dip angle is 60° and 65°.

For normal faults, the fault fracture zone is soft and easily becomes a stress release zone. The coal rock in the hanging wall near the fault plane slides along the fault fracture zone

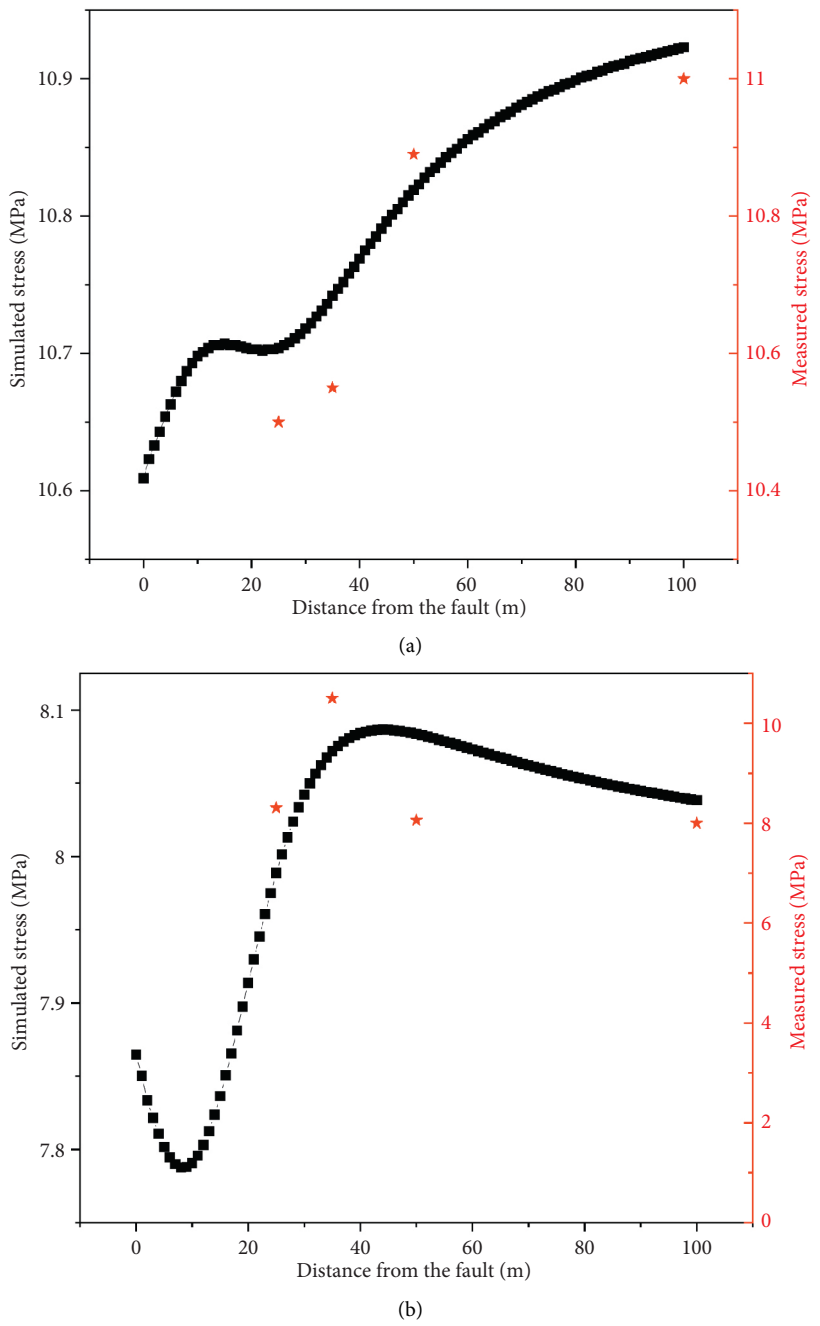

Figure 2: Comparison of measured and simulated values of horizontal stress (a) and vertical stress (b).

under the pressure of the overlying strata, resulting in compression deformation in the vertical direction. As a result, the coal rock at a certain distance from the fault exhibits a stress concentration zone due to the weak mechanical strength and vertical compression, while the coal rock close to the fault plane mainly exhibits a stress release zone due to its proximity to the pressure relief area of the fault fracture zone. Due to the deformation of the hanging wall, the movement of the coal rock in the footwall near the fault plane along the direction of the fault fracture zone is restricted, and no obvious compression deformation occurs in the vertical direction. Therefore, the coal rock in the footwall near the fault plane mainly exhibits a stress release zone due to its proximity to the pressure relief area of the fault fracture zone. In general, the k and D of the coal rock in the hanging wall of the normal fault are significantly larger than those in the footwall.

3.2. Influence of a Reverse Fault on the Stress of Coal Rock

3.2.1. Different Throws. Figure 5 shows the maximum principal stress distribution of the coal rock in the hanging wall and footwall of a reverse fault under different throws. The results show that the coal rock in the hanging wall has

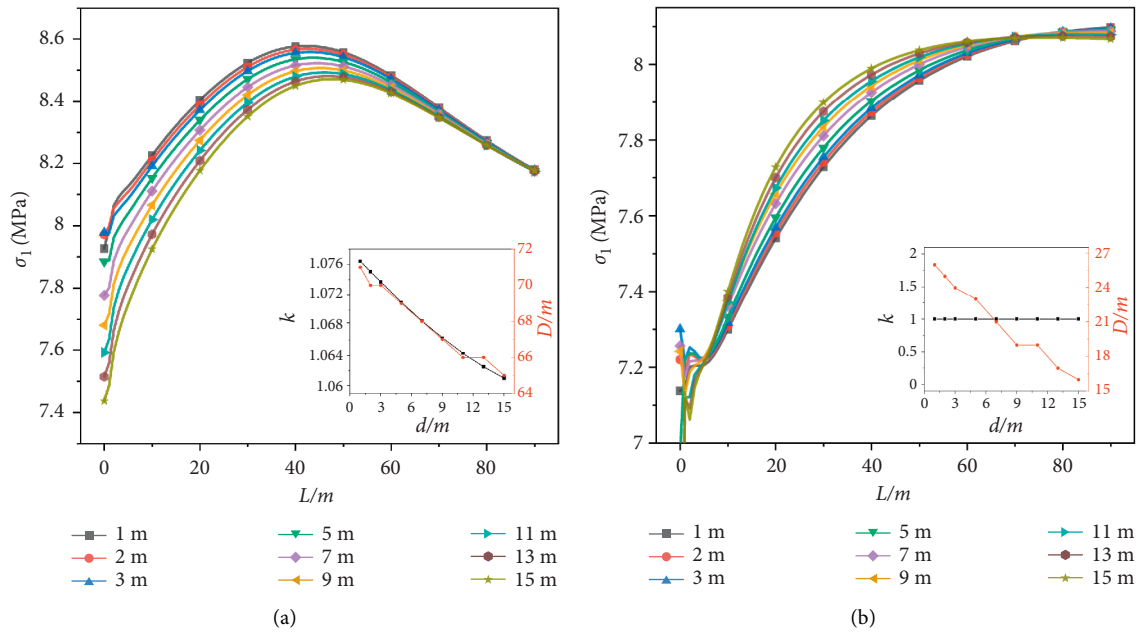

Figure 3: The stress distribution of the coal rock in the hanging wall (a) and footwall (b) of a normal fault under different throws.

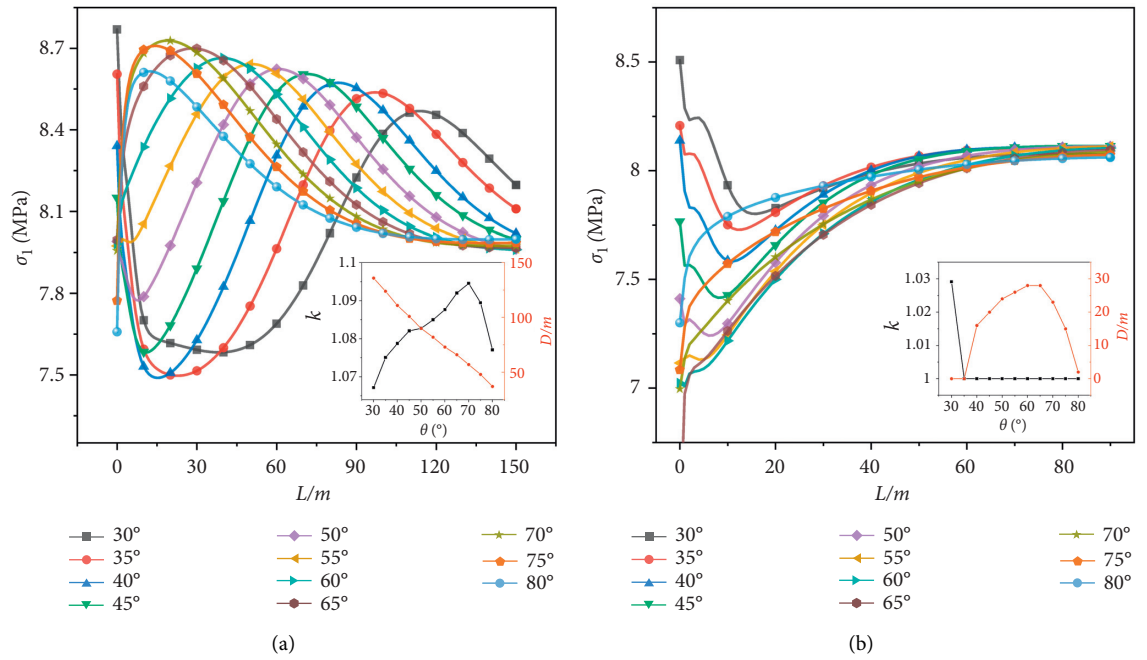

Figure 4: The stress distribution of the coal rock in the hanging wall (a) and footwall (b) of a normal fault under different dip angles.

mainly a high-stress gradient in the area within 30 m from the fault plane. When the throw gradually increases from 1 m to 7 m, the coal rock in the hanging wall produces a stress concentration zone within 10 m from the fault plane, and the k decreases with the increase in throw. When the throw continues to increase, the coal rock in the hanging wall mainly produces a stress release zone near the fault plane, which gradually increases to the original stress away from the fault. The D of the coal rock in the hanging wall is approximately 20 m near the fault plane and generally increases with an increasing throw. The stress distribution of the coal rock in the footwall is similar to that of the hanging wall, which will not be repeated here.

3.2.2. Different Dip Angles. Figure 6 shows the maximum principal stress distribution of the coal rock in the hanging wall and footwall of a reverse fault under different dip angles. The results show that the coal rock in the hanging wall has mainly a high-stress gradient in the area 30 m from the fault

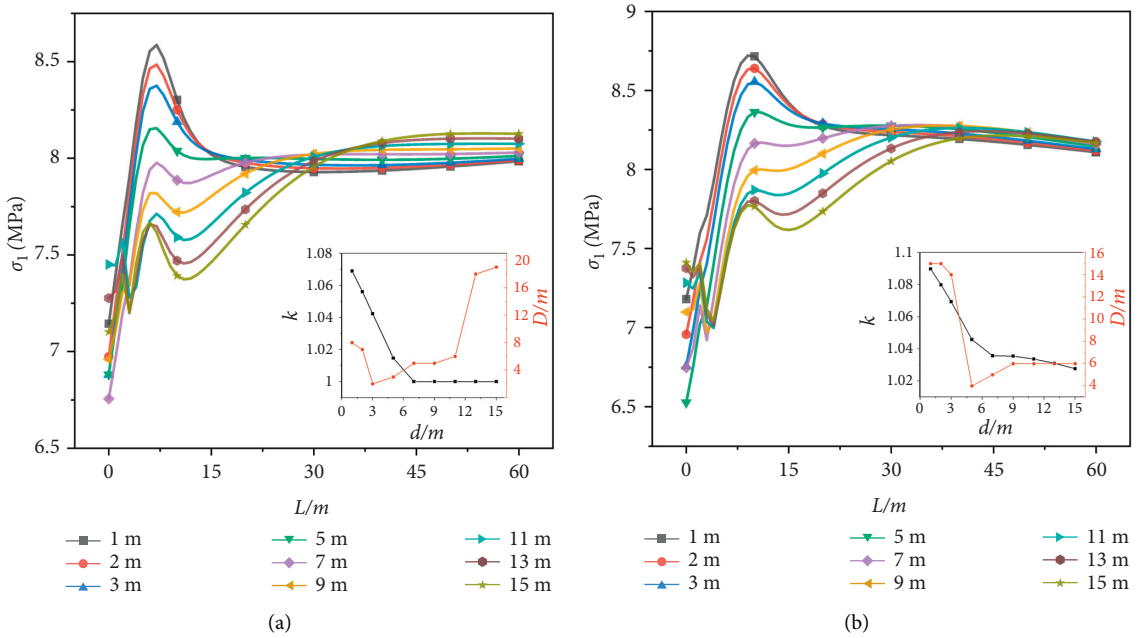

Figure 5: The stress distribution of the coal rock in the hanging wall (a) and footwall (b) of a reverse fault under different throws.

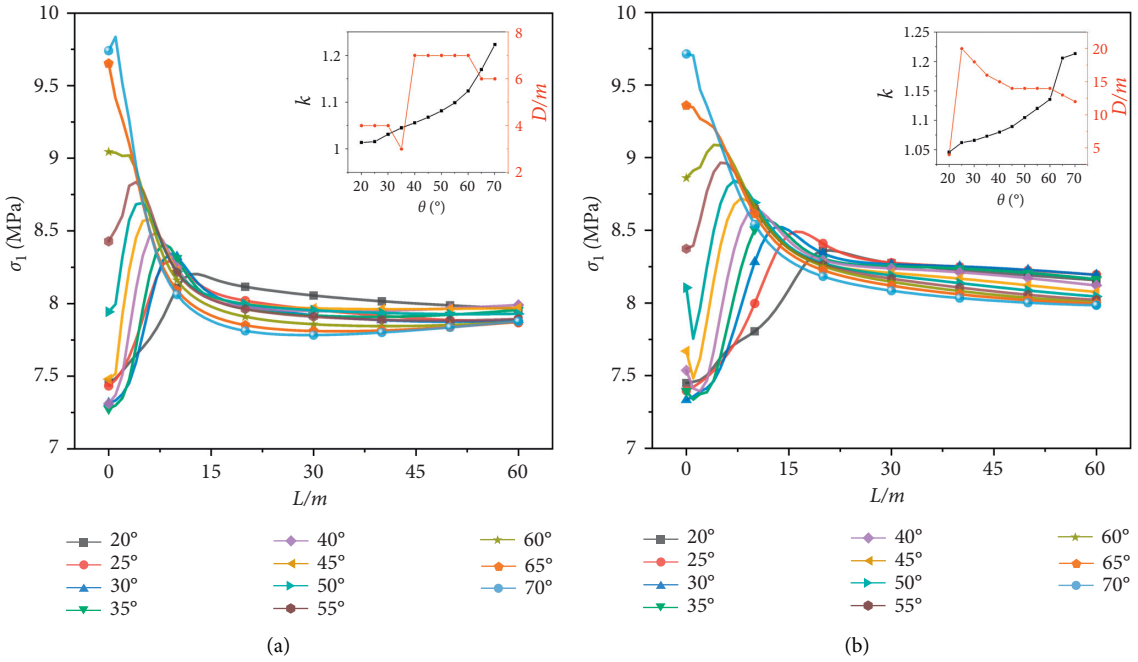

Figure 6: The stress distribution of the coal rock in the hanging wall (a) and footwall (b) of a reverse fault under different dip angles.

plane. Generally, the maximum principal stress shows a trend of first increasing and then decreasing away from the fault, and the stress release zone, the stress concentration zone, and the original stress zone appear in sequence. With the increase in the dip angle, the stress release zone of the coal rock in the hanging wall gradually shrinks until it disappears, while the stress concentration zone and the point corresponding to the maximum stress approach the fault plane. When the dip angle increases from 20° to 70°, the k of the coal rock in the hanging wall gradually increases from 1.05 to 1.21, and the D is approximately 20 m near the fault plane, which generally decreases with increasing dip angle. The stress distribution of the coal rock in the footwall is similar to that of the hanging wall, which will not be repeated here.

For reverse faults, the coal seam is supported by the hard roof and floor in the horizontal direction and has a low horizontal stress, so the maximum principal stress continues

to be dominated by the vertical stress. The hanging wall and footwall of the reverse fault move in opposite directions along the fault plane under the action of tectonic stress, but the surrounding rock hinders this deformation. As a result, the coal rock at a certain distance from the fault exhibits a stress concentration zone due to the weak mechanical strength and vertical compression, while the coal rock close to the fault plane mainly exhibits a stress release zone due to its proximity to the pressure relief area of the fault fracture zone. In general, the k and D of the coal rock in the footwall of the reverse fault are slightly larger than those of the hanging wall.

When the fault throw is small, it allows for more stress to transfer between the coal rock in the hanging wall and footwall, which forms a larger pressure relief zone together with the fault fracture zone, thus making the coal rock near the fault plane undergo greater deformation, and the k and D of the coal rock are relatively large. With the increase in fault throw, the stress transfer between the coal rock in the hanging wall and footwall is gradually weakened, so the k and D of the coal rock decrease accordingly. When the fault dip angle is relatively small, the D of the coal rock along the horizontal direction is larger, and the k of the coal rock is smaller due to the wider stress release zone. With the increase in the fault dip angle, the D of the coal rock along the horizontal direction gradually decreases, and the stress concentration zone gradually collapses to the fault plane, while the k of the coal rock gradually increases with the dip angle due to the shrinking of the stress release zone. Regardless of whether the fault present is a normal fault or reverse fault, the stress field of the coal rock shows this distribution characteristic.

4. The Prediction Model of the Tectonic Stress Field of a Fault-Containing Coal Rock

According to the above analysis, the functional relationship between the maximum principal stress of coal rock containing a fault and the related factors can be expressed as follows:

$$\sigma_1 = f\left(\sigma_0, L, d, \theta, W, N\right), \tag{1}$$

where W is the relative position of the fault where the coal rock is located ($W = 0$ when located on the hanging wall, $W = 1$ when located on the footwall), and N is the nature of the fault ($N = 0$ for normal faults, $N = 1$ for reverse faults).

For a certain engineering problem, $\sigma_0$at the far end of the fault is a fixed value, so the ratio of σ_1 to σ_0 is used instead of σ_1 to establish a functional relationship, and this ratio is named the stress coefficient λ as follows:

$$\lambda = f\left(L, d, \theta, W, N\right). \tag{2}$$

A supervised learning artificial neural network (ANN) is introduced to express the prediction model of the maximum principal stress of coal rock with a fault. The nonlinear mapping model between the stress coefficient of coal rock and its related factors is established. The input parameters were the L, d, θ, W, and N of coal rock with faults under various conditions. The output layer was the corresponding stress coefficient λ at each point.

In the prediction model, the relative position of each point from the fault and the fault parameters was transmitted forward to predict the stress coefficient, and the prediction error was transmitted backward to form a parameter adjustment closed loop, as shown in Figure 7. The loss function is shown as follows:

$$\text{loss} = -\frac{1}{n}\sum_{i=1}^{n}\left[\lambda_i \log \widehat{\lambda}_i + \left(1-\lambda_i\right)\log\left(1-\widehat{\lambda}_i\right)\right], \tag{3}$$

where n is the sample size and $\widehat{\lambda}$ and λ are the stress coefficient predicted value and the actual value, respectively.

The model training steps are as follows:

(1) Based on the foregoing numerical simulation results, the values of λ, L, d, θ, W, and N of several representative points of coal rock with faults under various conditions are obtained, and a total of 12080 sets of sample data are obtained.

(2) Organize training samples. The sample data are divided into a training set (90%) and a test set (10%) by random sampling. Taking L, d, θ, W, and N at each point to form the input vector and λ as the output vector, several sets of training samples of the artificial neural network are constructed.

(3) Neural network learning is done. Based on the learning of the fully connected artificial neural network model, the nonlinear mapping relationship model between λ and L, d, θ, W, and N of the coal rock is established. A threshold value is set, fitting parameters are adjusted, and the calculation is performed; this cycle is iterated until the accuracy requirements are met.

After model training, the error ε between the predicted value and the true value of λ at each point of the test set is shown in Figure 8, and 99% of the test samples have an error of less than 1%. Taking the coal rock in the hanging wall of a normal fault with a throw of 2 m and a dip angle of 65 as an example, a comparison between the predicted value and the true value of σ_1 is shown in Figure 9, and the fit between the two is good. These results show that the trained model can accurately express the nonlinear mapping relationship between the maximum principal stress of the coal rock and the related factors and has certain accuracy and reliability. For specific engineering problems, the predicted value of the stress coefficient and maximum principal stress can be obtained by inputting the related factors into the trained neural network model.

The prediction model of the fault-bearing tectonic stress field established in this study can effectively reflect the quantitative relationship between the stress of coal rock at various points near the fault and their spatial location and the fault property, throw, and dip angle. Compared to previously proposed models, the prediction model can provide guidance for the excavation design of mining engineering and early warning of possible coal and gas outburst

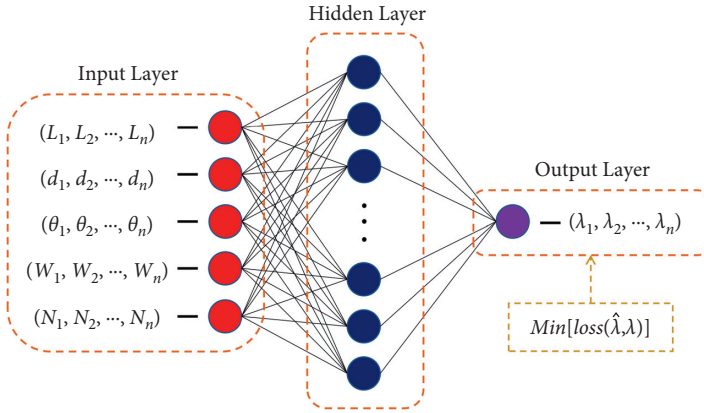

Figure 7: Structure diagram of ANN.

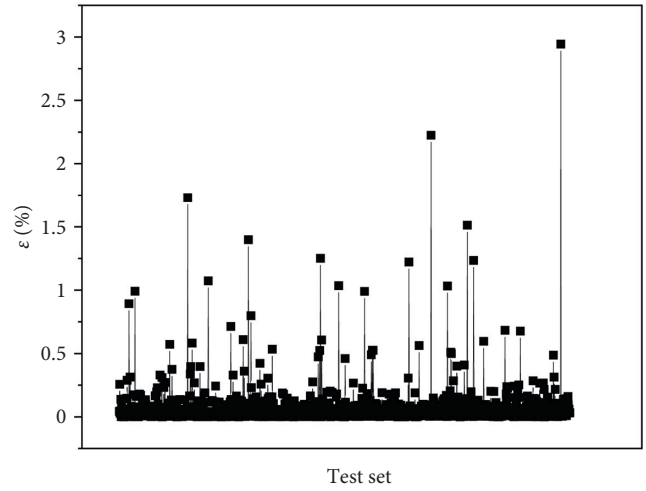

Figure 8: The error of the test set.

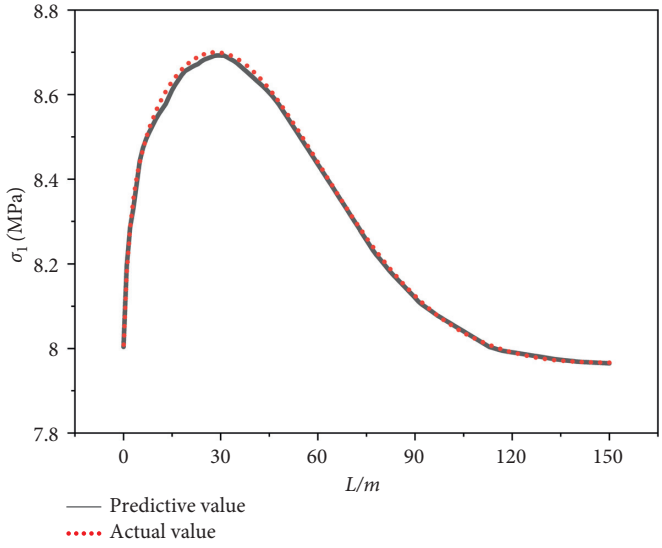

Figure 9: An application case of the prediction model.

disasters. Notably, the proposed prediction model still has certain limitations. For example, this study aims to revise the original stress σ_0 without considering geological factors in the critical energy equation of coal and gas outbursts. Thus, only the maximum principal stress of the coal rock is considered, and the shear stress of the coal rock and the mechanical properties of the roof and floor are not discussed and predicted. Furthermore, this study focuses on the distribution characteristics of the tectonic stress around small faults. Therefore, the ranges of the fault fracture zone extent and the fault throw magnitude have certain limitations. However, for preventing coal and gas outbursts in practice, even if a quantitative conclusion has certain errors and limitations, as long as it is within an acceptable range, it can also greatly promote the development of coal and gas outburst prevention technology. In addition, other similar problems may be encountered in underground geotechnical engineering (such as in the stability analysis of surrounding rocks, large fault zones, or folds), and the research ideas presented in this study can be used as a reference to construct more targeted training samples and training models to obtain a tectonic stress field prediction model more tailored to the project requirements.

5. Conclusions

In this study, a finite element model of a fault-containing coal rock *s* was established using numerical simulation methods to study the influence mechanisms of different fault parameters on the stress distribution characteristics of coal rock, and a prediction model of the tectonic stress field of a fault-containing coal rock was established based on the results of numerical simulations. The following main conclusions were drawn:

(1) The stress of the coal rock in the hanging wall of the normal fault is affected by the fault up to 100 m away from the fault, which is a significantly larger range of disturbance than that in the footwall of the normal fault and the hanging wall and footwall of the reverse fault, which are mainly up to 30 m from the fault plane.

(2) The coal rock in the hanging wall of the normal fault produces a stress concentration zone, but the change in the stress magnitude is limited. The stress concentration coefficient is less than 1.1 under the tested throw and dip angle conditions. The coal rock in the footwall of the normal fault mainly hosts the stress release zone. Both the hanging wall and the footwall of the reverse fault produce stress concentration zones, and the stress concentration degree of the footwall is greater than that of the hanging wall. When the dip angle is greater than 70°, the stress concentration coefficient of the coal rock in the footwall can exceed 1.2.

(3) With the increase in fault throw, the stress concentration factor and fault influence range both decrease. With the increase in fault dip angle, the stress concentration zone gradually collapses to the fault plane, and the stress concentration coefficient also gradually increases due to the reduction in the area of pressure relief. Regardless of whether the fault present is a normal fault or reverse fault, the stress field of the coal rock shows this distribution characteristic.

(4) Compared to previously proposed models, the prediction model of the tectonic stress field of a fault-containing coal rock established in this study can better describe the quantitative relationship between the fault parameters and the stress of coal rock, which can provide guidance for the excavation design of mining engineering and early warning of possible coal and gas outburst disasters.

Data Availability

Some or all data, models, or codes that support the findings of this study are available from the corresponding author upon reasonable request.

Conflicts of Interest

The authors declare that they have no conflicts of interest.

Acknowledgments

This work was supported by the National Natural Science Foundation of China (51874054) and the Major State Basic Research Development Program of China (2016YFC0801402).

References

[1] L. Wang, Y.-P. Cheng, and H.-Y. Liu, "An analysis of fatal gas accidents in chinese coal mines," *Safety Science*, vol. 62, pp. 107–113, 2014.

[2] X. Li, Z. Cao, and Y. Xu, "Characteristics and trends of coal mine safety development," *Energy Sources, Part A: Recovery, Utilization, and Environmental Effects*, vol. 2020, no. 12, pp. 1–19, 2020.

[3] X.-l. Li, S.-j. Chen, S.-m. Liu, and Z.-h. Li, "AE waveform characteristics of rock mass under uniaxial loading based on Hilbert-Huang transform," *Journal of Central South University*, vol. 28, no. 6, pp. 1843–1856, 2021.

[4] C. A. J. Wibberley, G. Yielding, and G. Di Toro, "Recent advances in the understanding of fault zone internal structure: a review," *Geological Society, London, Special Publications*, vol. 299, no. 1, pp. 5–33, 2008.

[5] B. Jiang, Y. Zhao, B. Lin, and T. Liu, "Effect of faults on the pore structure of coal and its resultant change on gas emission," *Journal of Petroleum Science and Engineering*, vol. 195, Article ID 107919, 2020.

[6] D. R. Faulkner, C. A. L. Jackson, R. J. Lunn et al., "A review of recent developments concerning the structure, mechanics and fluid flow properties of fault zones," *Journal of Structural Geology*, vol. 32, no. 11, pp. 1557–1575, 2010.

[7] F. H. An and Y. P. Cheng, "The effect of a tectonic stress field on coal and gas outbursts," *The Scientific World Journal*, vol. 2014, Article ID 813063, 10 pages, 2014.

[8] A.-u.-R. Maqbool, A. R. Moustafa, H. Dowidar, and M. Yousef, "Architecture of fault damage zones of normal

faults, Gebel Ataqa area, Gulf of Suez rift, Egypt," *Marine and Petroleum Geology*, vol. 77, pp. 43–53, 2016.

[9] Y. Zhao, L. Zhang, W. Wang, W. Wan, and W. Ma, "Separation of elastoviscoplastic strains of rock and a nonlinear creep model," *International Journal of Geomechanics*, vol. 18, no. 1, Article ID 04017129, 2018.

[10] H. Chu, X. Yang, C. Wang, and W. Liang, "Study on the coal damage and fracture mechanism under multiple actions of blasting stress wave," *Arabian Journal for Science and Engineering*, vol. 46, no. 11, pp. 10847–10854, 2021.

[11] S. Luo, P. Yan, W.-B. Lu et al., "Effects of in-situ stress on blasting damage during deep tunnel excavation," *Arabian Journal for Science and Engineering*, vol. 46, no. 11, pp. 11447–11458, 2021.

[12] X. Li, S. Chen, E. Wang, and Z. Li, "Rockburst mechanism in coal rock with structural surface and the microseismic (MS) and electromagnetic radiation (EMR) response," *Engineering Failure Analysis*, vol. 124, no. 3, Article ID 105396, 2021.

[13] S. Liu, X. Li, D. Wang, and D. Zhang, "Experimental study on temperature response of different ranks of coal to liquid nitrogen soaking," *Natural Resources Research*, vol. 30, no. 2, pp. 1467–1480, 2021.

[14] Y. Niu, Z. Li, B. Kong et al., "Similar simulation study on the characteristics of the electric potential response to coal mining," *Journal of Geophysics and Engineering*, vol. 15, no. 1, pp. 42–50, 2018.

[15] Y. Niu, C. Wang, E. Wang, and Z. Li, "Experimental study on the damage evolution of gas-bearing coal and its electric potential response," *Rock Mechanics and Rock Engineering*, vol. 52, pp. 4589–4604, 2019.

[16] W. Li, T. Ren, A. Busch et al., "Architecture, stress state and permeability of a fault zone in jiulishan coal mine, china: implication for coal and gas outbursts," *International Journal of Coal Geology*, vol. 198, pp. 1–13, 2018.

[17] M.-q. Huang, A.-x. Wu, Y.-m. Wang, and B. Han, "Geostress measurements near fault areas using borehole stress-relief method," *Transactions of Nonferrous Metals Society of China*, vol. 24, no. 11, pp. 3660–3665, 2014.

[18] P. Li, F. Ren, M. Cai, Q. Guo, and S. Miao, "Present-day stress state and fault stability analysis in the capital area of China constrained by in situ stress measurements and focal mechanism solutions," *Journal of Asian Earth Sciences*, vol. 185, Article ID 104007, 2019.

[19] L. R. Alejano, U. Castro-Filgueira, A. M. Ferrero, and M. R. Migliazza, "In situ stress measurement near fault and interpretation by means of discrete element modelling," *Acta Geodynamica et Geomaterialia*, vol. 14, no. 2, pp. 181–194, 2017.

[20] K. Matsuki, S. Nakama, and T. Sato, "Estimation of regional stress by FEM for a heterogeneous rock mass with a large fault," *International Journal of Rock Mechanics and Mining Sciences*, vol. 46, no. 1, pp. 31–50, 2009.

[21] P. Xu, "Geo-stress fields simulated with 3D FEM and their qualitative influence on coal and gas outburst," *Geotechnical & Geological Engineering*, vol. 32, no. 2, pp. 337–344, 2014.

[22] Y. Shan, Z. Li, and G. Lin, "A stress inversion procedure for automatic recognition of polyphase fault/slip data sets," *Journal of Structural Geology*, vol. 26, no. 5, pp. 919–925, 2004.

[23] B. Chen, Q. Ren, and F. Wang, Y. Zhao, Inversion analysis of in-situ stress field in tunnel fault zone considering high geothermal," *Geotechnical & Geological Engineering*, vol. 39, no. 4, 2021.

[24] D. Y. Xu, Q. T. Hu, and H. Si, "Measurement and inversion of the stress distribution in a coal and rock mass with a fault," *International Journal of Geomechanics*, vol. 21, no. 11, 2021.

[25] S. A. Kattenhorn and S. T. Marshall, "Fault-induced perturbed stress fields and associated tensile and compressive deformation at fault tips in the ice shell of Europa: implications for fault mechanics," *Journal of Structural Geology*, vol. 28, no. 12, pp. 2204–2221, 2006.

[26] P. J. Lovely, D. D. Pollard, and O. Mutlu, "Regions of reduced static stress drop near fault tips for large strike-slip earthquakes," *Bulletin of the Seismological Society of America*, vol. 99, no. 3, pp. 1691–1704, 2009.

[27] F. A. Livio, M. F. Ferrario, C. Frigerio, A. Zerboni, and A. M. Michetti, "Variable fault tip propagation rates affected by near-surface lithology and implications for fault displacement hazard assessment," *Journal of Structural Geology*, vol. 130, Article ID 103914, 2020.

[28] T. Suzuki and T. Yamashita, "Nonlinear effects of temperature, fluid pressure, and inelastic porosity on dynamic fault slip and fault tip propagation: emergence of slip strengthening and pulse-like fault slip," *Journal of Geophysical Research*, vol. 113, no. B7, Article ID B07304, 2008.

[29] Y. Kang, Q. Liu, and H. Xi, "Numerical analysis of THM coupling of a deeply buried roadway passing through composite strata and dense faults in a coal mine," *Bulletin of Engineering Geology and the Environment*, vol. 73, no. 1, pp. 77–86, 2014.

[30] Y. Wang, H. Jing, H. Su, and J. Xie, "Effect of a fault fracture zone on the stability of tunnel-surrounding rock," *International Journal of Geomechanics*, vol. 17, no. 6, Article ID 04016135, 2017.

[31] Y. Xing, P. H. S. W. Kulatilake, and L. A. Sandbak, "Stability assessment and support design for underground tunnels located in complex geologies and subjected to engineering activities: case study," *International Journal of Geomechanics*, vol. 19, no. 5, Article ID 05019004, 2019.

[32] H. Wang, R. Shi, D. Deng, Y. Jiang, G. Wang, and W. Gong, "Characteristic of stress evolution on fault surface and coal bursts mechanism during the extraction of longwall face in Yima mining area, China," *Journal of Structural Geology*, vol. 136, Article ID , 2020.

[33] T. Li, Z. Mu, G. Liu, J. Du, and H. Lu, "Stress spatial evolution law and rockburst danger induced by coal mining in fault zone," *International Journal of Mining Science and Technology*, vol. 26, no. 3, pp. 409–415, 2016.

[34] F. Gao, H. Kang, and J. Li, "Numerical simulation of fault-slip rockbursts using the distinct element method," *Tunnelling and Underground Space Technology*, vol. 110, Article ID 103805, 2021.

[35] B.-H. Kim and M. K. Larson, "Development of a fault-rupture environment in 3D: a numerical tool for examining the mechanical impact of a fault on underground excavations," *International Journal of Mining Science and Technology*, vol. 29, no. 1, pp. 105–111, 2019.

[36] X. Li, S. Chen, Q. Zhang, X. Gao, and F. Feng, "Research on theory, simulation and measurement of stress behavior under regenerated roof condition," *Geomechanics and Engineering*, vol. 26, no. 1, pp. 49–61, 2021.

[37] L. Chen, B. Shen, and B. Dlamini, "Effect of faulting on coal burst-a numerical modelling study," *International Journal of Mining Science and Technology*, vol. 28, no. 5, pp. 739–743, 2018.

[38] C. Lin, D. Guo, and Y. Liang, "Influence of structural elements and stress on mining-induced fault slip," *Geotechnical & Geological Engineering*, vol. 36, no. 1, pp. 439–453, 2018.

[39] A. Tajdus, M. Cala, and K. Tajdus, "The influence of normal fault on initial state of stress in rock mass," *Studia Geotechnica et Mechanica*, vol. 38, no. 1, pp. 107–119, 2016.